Carbohydrate Polymers 99 (2014) 180–189

Contents lists available at ScienceDirect

Carbohydrate Polymers

journal homepage: www.elsevier.com/locate/carbpol

Purification, characterization and comparative studies of spray-dried bacterial cellulose microparticles

Mohd Cairul Iqbal Mohd Amin*, Abadi Gumah Abadi, Haliza Katas

Centre for Drug Delivery Research, Faculty of Pharmacy, Universiti Kebangsaan Malaysia, Jalan Raja Muda Abdul Aziz, Kuala Lumpur 50300, Malaysia

ARTICLE INFO

Article history:
Received 27 April 2013
Received in revised form 16 August 2013
Accepted 16 August 2013
Available online 22 August 2013

Keywords:
Bacterial cellulose
Powder
Spray drying
Flowability

ABSTRACT

Bacterial cellulose (BC) is a biopolymer with significant potential for the development of novel materials. This work aimed to prepare and characterize BC powders from *nata de coco*, and assess the possible enhancement of the powder properties by spray drying. Therefore, BC powders prepared by acid treatment and mechanical processing were spray-dried, and characterized according to their morphology, flowability, thermal stability, water retention capacity, and compared with commercial microcrystalline cellulose (MCC). The powders redispersibility and suspensions rheology were also evaluated. SEM showed that spray-dried BC microparticles exhibited semispherical shape and had flow rate of 4.23 g s^{-1} compared with 0.52 g s^{-1} for MCC. Particle size analysis demonstrated that spray-dried BC microparticles could be redispersed. TGA showed that BC samples had higher thermal stability than MCC. Water retention capacities of BC samples were greater than MCC. These findings provide new insight on the potential applications of spray-dried BC as a promising pharmaceutical excipient.

1. Introduction

Recently, biomaterials have attracted significant attention in search for materials with characteristic features of renewability, sustainability, and biocompatibility (Klemm et al., 2006). Cellulose is the most abundant natural, renewable, biodegradable, and biocompatible polymer. In addition to plants, cellulose is also secreted extracellularly by some bacterial species, particularly *Acetobacter* strains, known as bacterial cellulose (BC) or microbial cellulose (Panesar, Chavan, Chopra, & Kennedy, 2012). Although it is chemically equivalent to plant cellulose, BC has distinct ultrafine fibrils of nanosized three-dimensional network structure, and possess superior properties compared to plant cellulose (George & Siddaramaiah, 2012). Owing to its fascinating properties including renewability, low toxicity, biocompatibility, ability to form micro- and nanoparticles, stability, and compatibility with a wide range of actives, cellulose has attracted a lot of attention for utilization in a variety of applications (Edgar, 2007; Klemm et al., 2006). Cellulose micro- and nanoparticles are usually prepared through the disintegration of native cellulose, and has been frequently attained by several methods. These include mechanical methods, which utilize force mediated by a high-pressure homogenizer or a microfluidizer (Eyholzer, Bordeanu, Lopez-Suevos, Rentsch, Zimmermann, & Oksman, 2010), hydrolysis with mineral acid solutions, or using enzymes (George, Ramana, & Bawa, 2011; Peng, Gardner, & Han, 2012), and microbial activities (Satyamurthy, Jain, Balasubramanya, & Vigneshwaran, 2011). Ionic liquids have recently been considered as potential solvents for cellulose dissolution because they have low vapor pressure, non-flammable, and are thermally and chemically stable (Heinze, Schwikal, & Barthel, 2005; Lan, Liu, Yue, Sun, & Kennedy, 2011).

Cellulose is generally processed as an aqueous suspension. To mitigate the drawbacks of producing cellulose in aqueous suspensions, such as high shipping costs, requirement of large storage facilities, and its propensity for microbial decomposition, the suspensions are usually dried before further usage (Eyholzer et al., 2010; Peng et al., 2012). Among the various drying techniques for obtaining dried particles from suspensions or solutions, freeze drying and spray drying are the most commonly employed methods in diverse industries to obtain products with specific properties and to ensure the stability of products (Paudel, Worku, Meeus, Guns, & Van den Mooter, 2013; Peng et al., 2012). Spray drying is a versatile technique that offers several advantages over extensively used freeze drying: it allows rapid heat and mass transfer in a continuous mode; eliminates post-processing stages such as grinding and screening; it increases the sterility of the product; and high-quality powders can be produced by engineering the size, shape, and morphology of particles (Paudel et al., 2013; Peng et al., 2012). End-product characteristics such as particle size, particle morphology, moisture content, and bulk density are influenced by process parameters including inlet temperature, atomizing air flow rate,

* Corresponding author. Tel.: +60 3 9289 7690; fax: +60 3 2698 3271.
E-mail addresses: mciamin@pharmacy.ukm.my, mciamin@yahoo.co.uk (M.C.I.M. Amin).

0144-8617/$ – see front matter © 2013 Elsevier Ltd. All rights reserved.
http://dx.doi.org/10.1016/j.carbpol.2013.08.041

and pressure, and feed variables such as feed rate and feed concentration. A major advantage of spray drying over other drying methods is that it allows the control of these variables; this is especially useful when dealing with high-value products such as pharmaceuticals (Cal & Sollohub, 2010; Walton & Mumford, 1999).

The preparation of cellulose micro- and nanoparticles has provided abundant opportunities for the development of innovative materials (Kolakovic, Laaksonen, Peltonen, Laukkanen, & Hirvonen, 2012; Peng et al., 2012). Given its superior properties compared to plant cellulose, BC has been extensively investigated and utilized in several applications such as food products, biomedical applications, drug delivery systems, and biocomposites (Czaja, Krystynowicz, Bielecki, & Brown, 2006; Klemm et al., 2006; Müller et al., 2013). We previously investigated the applications of BC as a film-coating agent and hydrogel former (Amin & Abadi, 2012; Halib, Amin, & Ahmad, 2010; Halib & Amin, 2012). In this study, BC was prepared from a readily available foodstuff, *nata de coco*, and the possibility of improvement in the powder properties by spray drying and acid treatment was examined. The prepared BC powders were then compared with MCC. Further, the effects of acid treatment and spray drying on the morphology, crystallinity, thermal stability, flowability, water retention capacity, and rheological properties of BC suspensions were also investigated.

2. Materials and methods

2.1. Materials

BC (*nata de coco*, a foodstuff) was purchased from a local food industry; Avicel PH101 NF Lot P110821447 from FMC, USA, and assigned as MCC; sodium hydroxide from J.T. Baker, Sweden; and 85% phosphoric acid from R&M Marketing Essex, UK.

2.2. Preparation of BC powders

Crude *nata de coco* was purified by washing with distilled water several times, blended using a conventional laboratory blender at 2000 rpm for 5 min, then treated with 1 N NaOH solution at 90 °C for 1 h, washed with distilled water several times until neutrality and was labeled purified BC.

A portion of purified BC was freeze-dried using a bench top freeze dryer, Coolsafe-110 (ScanVac, Denmark), at −110 °C for 48 h. The dry samples thus obtained were micronized by a variable-speed rotor mill (Pulverisette14; Fritsch, Germany) and fractionated on a sieve shaker (Endecott, UK). The particle size fraction of ≤50 μm was collected and assigned as MBC (microfine BC).

For preparation of BC by acid treatment, the required amount of purified BC was blended for 20 min at 5000 rpm, mixed with phosphoric acid in the ratio of 1:5 (w/v), and allowed to hydrolyze at 60 °C for 2 h. Hydrolysis was terminated by pouring the slurry into distilled water with continuous mechanical stirring for 0.5 h. The suspension was subjected to several centrifugation and washing cycles with deionized purified water at 10,000 rpm and 5 °C for 20 min until neutrality and was labeled purified acid-treated BC. Further, a portion of purified acid-treated BC was lyophilized, micronized, and assigned as ABC (acid-treated BC), while the other portion was later used for spray drying.

For preparation of spray-dried powders, the non-lyophilized portion of purified acid-treated BC was diluted to 1% (w/v) in distilled water and mechanically homogenized for 1 h. Moreover, a 1% (w/v) MBC suspension was prepared by mixing the required amount with distilled water and homogenized for 1 h. The suspensions (volumes of 5 L) were spray-dried using a B290 mini spray dryer (Buchi, Switzerland), operated at 190 °C inlet temperature, 100 °C outlet temperature, 95% aspiration, and 10% spray rate. The spray-dried powders were assigned as MSD (microfine spray-dried BC) and ASD (acid-treated spray-dried BC).

2.3. Fourier transform infrared spectroscopy (FT-IR)

FT-IR spectra of MBC, MSD, ABC, ASD, and MCC were recorded using a Spectrum100 Fourier transform infrared spectrometer (PerkinElmer, USA) utilizing the KBr technique (range: 4000–400 cm^{-1}, resolution: 4 cm^{-1}, and number of accumulation scans: 16). The spectra were baseline-corrected and optimized using Spectrum software. Crystallinity index (CIir) was measured as the ratio of the absorption bands 1430/900. Cellulose Iα fraction was estimated using the following equation:

$$\int_{\alpha} ir = \frac{A750}{A750 + A710} \quad (1)$$

where $A750$ and $A710$ are the absorbance intensities of Iα and Iβ respectively, at the corresponding wavenumbers.

2.4. X-ray diffraction (XRD) analysis

XRD patterns of the samples were acquired using a D8 Discovery diffractmeter (Bruker AXS, Germany) using nickel-filtered Cu Kα radiation (λ = 1.5406 Å) at 40 kV, 40 mA, angular scanning (2θ) of 5–40°, and step size of 0.02°. The crystallinity indices (CrI) were determined using the Segal equation:

$$\mathrm{CrIxrd} = \frac{I_{0\ 0\ 2} - I_{\mathrm{am}}}{I_{0\ 0\ 2}} \times 100 \quad (2)$$

where I_{002} is the peak intensity at the (0 0 2) (2θ = 22.5°) plane, and I_{am} is the minimum intensity at the valley between (0 0 2) and (1 0 1) planes (2θ = 18°).

The *d*-spacings between crystal planes at the main peaks were determined using the Bragg's law:

$$\lambda = 2d \quad \sin \quad \theta \quad (3)$$

where d is the distance between the crystal planes, θ is the Bragg angle, and λ the X-ray wavelength.

To categorize the samples as Iα-rich or Iβ-rich, the empirical equation developed by Wada, Okano, and Sugiyama (2001) was employed:

$$Z = 1693d_1 - 902d_2 - 549 \quad (4)$$

where d_1 is the *d*-spacing of peak 1 and d_2 is the *d*-spacing of peak 2.

The crystallite sizes CS_1, CS_2, and CS_3 at the main peaks 1 0 1, $1\ 0\ \bar{1}$, and 0 0 2, respectively, were determined using the Scherrer equation:

$$\mathrm{CS} = \frac{0.9\lambda}{H \quad \cos \quad \theta} \quad (5)$$

where CS is the crystallite size, λ is the X-ray wavelength, H is the full-width at half-maximum (FWHM), and θ is the Bragg angle at the corresponding lattice plane.

2.5. Scanning electron microscopy (SEM)

The particle morphology was examined using a scanning electron microscope (VP1450; Leo, UK). The powders were mounted on aluminum stubs, coated with gold for 120 s with a sputter coater (SC500; BioRad, UK) under an argon atmosphere, and observed at an acceleration voltage of 15 kV.

2.6. Thermogravimetric analysis (TGA)

The thermal stability of the samples was evaluated using a thermal analyzer (STA6000; Perkin Elmer, US). Samples of 10 mg were scanned from 50 to 600 °C at a rate of 10 °C/min under nitrogen flow. The moisture content was calculated as the percentage of weight loss upon heating after holding the samples at 125 °C for 5 min.

2.7. Rheological studies and particle size analysis

Suspensions of MBC, MSD, ABC, and ASD were prepared by mixing the required amount of powders to produce aqueous suspensions of the intended concentration in 500 ml of distilled water. The suspensions were mechanically stirred for 4–5 h and were then sonicated for 5 min. The viscosity and rheological properties of the suspensions were measured by a programmable digital viscometer (DV-III Ultra Rheometer; Brookfield Engineering, US) using a cylindrical LV1 spindle. The viscosities were tested in the temperature range 25–60 °C. For rheological studies, the samples were tested at shear rates of 10–30 rpm at 25 °C. All data were measured in triplicates at torque values greater than 10%.

The particle size distribution of the powders was determined by laser diffractometer (Mastersizer 2000; Malvern, UK) equipped with a Hydro MU2000 unit. The required quantities of MBC, MSD, ABC, and ASD to prepare 1% (w/v) suspensions were mixed with distilled water, and mechanically homogenized for 1 h. The suspensions were added to a dispersing unit containing 700 ml of distilled water stirred at 2000 rpm until the concentration was sufficient to achieve an obscuration of 12–15%. The volume diameters $d(0.1)$, $d(0.5)$, and $d(0.9)$ were averaged from 5 measurements. The polydispersity index (PDI) of each sample was represented by the distribution span and calculated using the equation given by Kumar, Sharma, and Pathak (2013).

$$\text{Span} = \frac{d(0.9) - d(0.1)}{d(0.5)} \tag{6}$$

where $d(0.1)$, $d(0.5)$, and $d(0.9)$ represent 10%, 50%, and 90% of the total measured volume of particles, respectively.

2.8. Powder density and porosity

A known quantity of the powders was gently introduced into a 250-ml graduated cylinder, and the ratio of mass to volume was referred to as bulk density (g/ml). For the determination of tapped density, the cylinder was placed on an automatic tapper (AUTOTAP; Quantachrome Instruments, US) and mechanically tapped 1200 times. The powder volume after tapping was subsequently used to calculate the tapped density (g/ml). All values were averaged from 3 measurements.

The true density of the powders was determined using a helium pycnometer (Ultrapycnometer 1000; Quantachrome, US). The powders were oven-dried at 105 °C for 3 h or until there was no further change in weight before testing. Samples of 1.0 g were analyzed in triplicate.

The porosity was determined using the following equation:

$$\varepsilon = \frac{1 - \rho_{\text{tap}}}{\rho_{\text{true}}} \times 100 \tag{7}$$

where ε, ρ_{tap}, and ρ_{true}, are the porosity, tapped density, and true density of the powder, respectively.

2.9. Powder flowability

The compressibility index (CI) and Hausner ratio (HR) of the powders were calculated using the following equations:

$$\text{CI} = \frac{[\rho_{\text{tap}} - \rho_{\text{bulk}}]}{\rho_{\text{tap}}} \times 100 \tag{8}$$

$$\text{HR} = \frac{\rho_{\text{tap}}}{\rho_{\text{bulk}}} \tag{9}$$

where ρ_{tap} and ρ_{bulk} are tapped and bulk density of the powder, respectively.

The angle of repose of the powders was measured by the fixed height method. For this, a funnel with an orifice 15 mm in diameter was secured at a height of 20 cm from a flat stable surface. Samples of similar weight were filled into the funnel and allowed to fall, and the mean radius and height of the obtained conical pile were measured. The angle of repose was then calculated using the following formula:

$$\tan\ \alpha = \frac{h}{r} \tag{10}$$

where α is the angle of repose, h is the height of the conical pile, and r is the mean radius of the conical pile.

The flow rate was determined by filling the funnel with 50 g of a powder and measuring the time of flow through the orifice. The values were averaged from 3 measurements.

2.10. Water retention capacity (WRC) and swelling index (SI)

The swelling index of the powders was determined by measuring the volume occupied by the powders before and after swelling. Samples of 1.0 g were placed in 25 ml measuring cylinders, and the dry sample volume was noted. Then, 25 ml of distilled water was added. The vessel was shaken every 10 min for 1 h and allowed to stand for 3 h, and the increase in volume was measured. The swelling index was expressed as ml/g of the dry weight.

For measuring the water retention capacity (WRC) of the powders, 1.0 g samples were quantitatively transferred into test tubes and weighed (w_1). Then, 10 ml of distilled water was added to each sample and mixed for 1 min. The samples were allowed to stand at 25 °C for 30 min, centrifuged at 4000 × g for 15 min, and then drained by tilting the test tubes approximately 10° from the horizontal for 10 min. The test tubes were weighed (w_2), and the water retained was calculated as follows:

$$\text{WRC} = \frac{w_2 - w_1}{w_1} \tag{11}$$

WRC was expressed as the weight of water retained per gram of dry powder.

2.11. Statistical analysis

The data were expressed as mean ± standard deviation (SD) and evaluated by one-way analysis of variance (ANOVA) followed by Tukey's test. P-values less than 0.05 ($P < 0.05$) were regarded as significant. All statistical analyses were carried out using SPSS for Windows, Version 16.0 (IBM Corporation, US).

3. Results and discussion

3.1. FT-IR analysis

The FT-IR spectra of MBC, MSD, ABC, ASD, and MCC are shown in Fig. 1. The powders displayed similar main characteristic peaks representative of cellulose I allomorph. The peaks around 3349 cm^{-1}

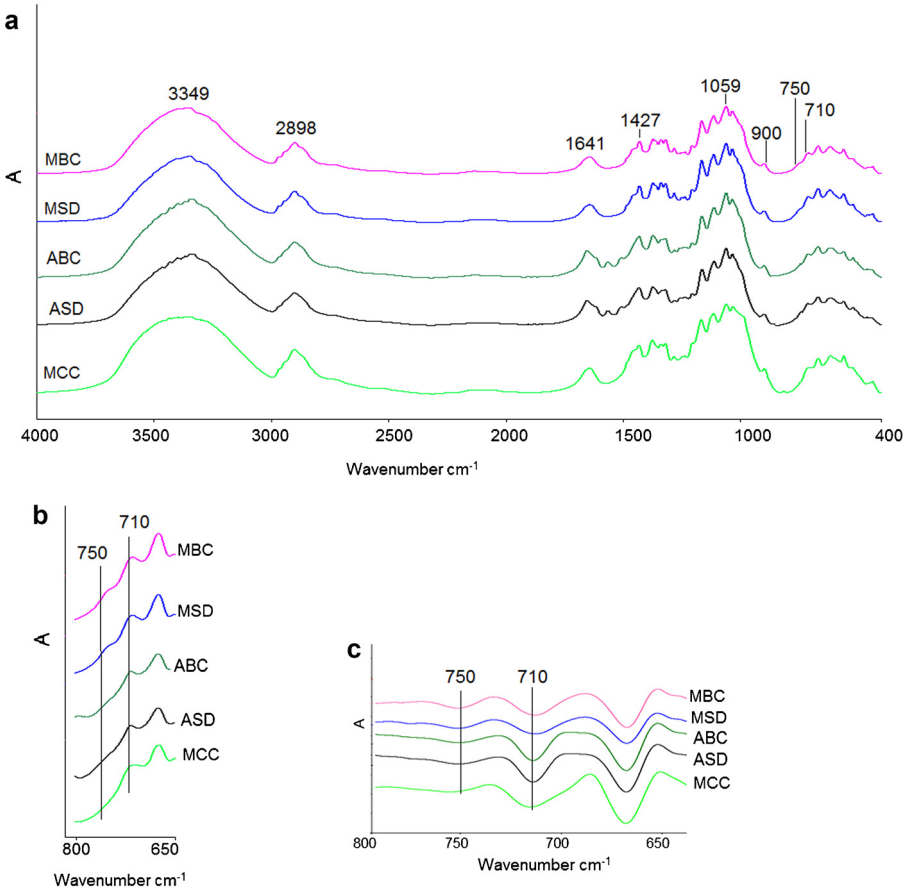

Fig. 1. (a) FT-IR spectra, (b) enlarged FT-IR spectra, and (c) enlarged second derivative FT-IR spectra of microfine BC (MBC), spray-dried microfine BC (MSD), acid-treated BC (ABC), acid-treated spray-dried BC (ASD), and MCC.

were attributed to OH stretching vibrations. Further, the absorption bands at 2898, 1641, 1427, and 1059 cm^{-1} were attributed to C—H stretching of —CH_2, O—H bending of adsorbed water, —CH_2 symmetric bending, and C—O—C pyranose ring skeletal vibrations, respectively. The crystallinity index (CIir) was estimated from the absorbance ratio of the bands 1427/900 cm^{-1} as these bands are sensitive to the relative amount of crystalline and amorphous phases (Yan, Chen, Wang, Wang, & Jiang, 2008). As shown in Table 1, ABC and ASD displayed significantly ($P < 0.05$) higher CIir than MBC, MSD, and MCC. However, MCC showed slightly higher CIir than MBC and MSD. The higher CIir of ABC, ASD, and MCC were due to preferential hydrolysis of amorphous and less-ordered regions by acid.

Cellulose produced in nature is a composite of two distinct allomorphs: one-chain triclinic and two-chain monoclinic unit cells, namely, Iα and Iβ, respectively (Atalla & Vanderhart, 1984; Wada & Okano, 2001). Iα content was estimated from FT-IR. The results are presented in Table 1. MBC and MSD showed an Iα fraction of about 0.32, which was in agreement with reported data (Ul-Islam, Shah, Ha, & Park, 2011). It has been reported that BC microstructural properties such as crystallinity, crystallite size, Iα fraction, and mechanical properties depend on the organism from which BC is obtained, as well as on growth conditions including culture medium composition, fermentation conditions, incubation time, inoculum volume, surface area, and media volume (Dayal, Goswami, Sahai, Jain, Mathur, & Mathur, 2013; Ruka, Simon, & Dean, 2012). Fig. 1 shows the FT-IR spectra of the samples (Fig. 1a), an enlarged view of the spectra (Fig. 1b), and an enlarged view of second derivatives of the spectra (Fig. 1c). It can be observed that all samples showed reliable peaks at 710 cm^{-1}, attributed to the contribution of Iβ. However, the intensities of the peaks for MCC, ABC, and ASD were relatively higher than those for MBC and MSD. In contrast, the peaks at 750 cm^{-1}, attributed to the contribution of Iα, MCC, ABC, and ASD showed lesser intensities than those for MBC

Table 1
FT-IR crystallinity index (CIir), Cellulose Iα fraction (f_αIR), *d*-spacings (d_1, d_2 and d_3), *z*-value, crystallite sizes (CS_1, CS_2 and CS_3) and XRD crystallinity index (CrIxrd) of microfine BC (MBC), spray-dried microfine BC (MSD), acid treated BC (ABC), acid treated spray-dried BC (ASD) and MCC.

	CIir	f_αIR	d_1 (nm)	d_2 (nm)	d_3 (nm)	*z*-Value	CS_1 (nm)	CS_2 (nm)	CS_3 (nm)	CrIxrd (%)
MBC	2.14 ± 0.012	0.328 ± 0.004	0.612[a] ± 0.002	0.532[a] ± 0.002	0.393 ± 0.001	7.25	5.40 ± 0.002	6.33 ± 0.002	5.83[a] ± 0.002	75.3 ± 3.5
MSD	2.08[a] ± 0.021	0.323 ± 0.007	0.612[a] ± 0.002	0.532[a] ± 0.001	0.394 ± 0.002	7.25	5.40 ± 0.001	6.33 ± 0.002	5.83[a] ± 0.002	73.7 ± 2.1
ABC	2.36[a,b] ± 0.012	–	0.608[a,b] ± 0.001	0.537[a,b] ± 0.002	0.394 ± 0.002	−4.03	5.32[b] ± 0.002	6.28[b] ± 0.002	5.71[a,b] ± 0.001	85.1[a,b] ± 4.7
ASD	2.31[a,c] ± 0.020	–	0.608[a,c] ± 0.002	0.537[a,c] ± 0.002	0.393 ± 0.001	−4.03	5.32[c] ± 0.002	6.28[c] ± 0.001	5.71[a,c] ± 0.002	82.6[a,c] ± 2.8
MCC	2.18 ± 0.018	–	0.603 ± 0.002	0.538 ± 0.002	0.394 ± 0.002	−13.4	–	–	5.53 ± 0.001	77.8 ± 2.4

Data are means ± SD ($n = 3$), $P < 0.05$.
[a] Statistically showed significant difference for MBC, MSD, ABC and ASD vs MCC.
[b] Statistically showed significant difference for ABC vs MBC.
[c] Statistically showed significant difference for ASD vs MSD.

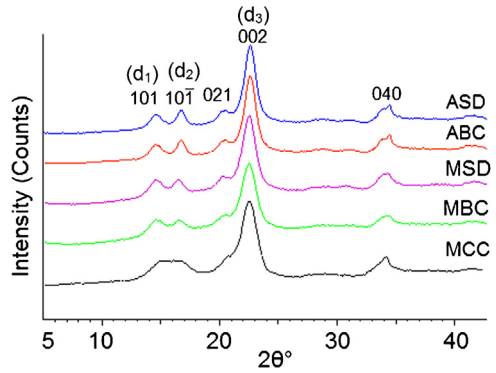

Fig. 2. XRD diffractograms of microfine BC (MBC), spray-dried microfine BC (MSD), acid-treated BC (ABC), acid-treated spray-dried BC (ASD), and MCC.

and MSD. The reduced Iα peak intensities for ABC and ASD samples as compared to their predecessors suggests that Iα was reduced by the acid treatment. This is because Iα is metastable, more reactive and more selectively degraded than Iβ (Hayashi, Sugiyama, Okano, & Ishihara, 1997; Wada & Okano, 2001).

3.2. XRD analysis

XRD patterns of the samples are shown in Fig. 2. The powders displayed similar characteristic peaks at 2θ of 14.5°, 16.5°, and 22.5°. These diffractions were ascribed to the crystallographic planes 1 0 1, 1 0 $\bar{1}$, and 0 0 2, respectively (Lee & Bismarck, 2012; Tomé et al., 2010). A peak at 34.52° and a shoulder at 20.6° ascribed to the 0 4 0 and 0 1 2 lattice plane reflections, respectively, can also be observed (Hult, Iversen, & Sugiyama, 2003). These diffractions correspond to the typical profile of the cellulose I allomorph (Hult et al., 2003; Park, Baker, Himmel, Parilla, & Johnson, 2010). The crystallinity index values of the samples are listed in Table 1. All samples possessed high crystallinity; however, MBC and MSD exhibited significantly ($P<0.05$) lower crystallinity than ABC and ASD, and slightly ($P>0.05$) lower crystallinity than MCC. Further, ABC and ASD demonstrated significantly ($P<0.05$) higher crystallinity than MCC. The high crystallinity of MCC, ABC, and ASD is due to the acid treatment, as the acid preferably hydrolyzed the amorphous and less-ordered regions of cellulose. MSD and ASD demonstrated slightly insignificant ($P>0.05$) lower crystallinity than their precursors. These results are in accordance with literature data, suggesting that the rapid evaporation of water during spray drying limits the chain mobility of cellulose, and consequently, its alignment, which decreases the crystallinity (Rojas & Kumar, 2011a).

It has been reported that the *d*-spacing data reflect the ratio of Iα and Iβ. Each peak corresponds to contributions from both Iα and Iβ diffractions whose *d*-spacings are slightly different: d_1 is Iα 1 0 0 and Iβ 1 $\bar{1}$ 0; d_2 is Iα 0 1 0 and Iβ 1 1 0; and d_3 is Iα 1 1 0 and Iβ 2 0 0 (Wada & Okano, 2001; Wada, Okano, & Sugiyama, 2001). Table 1 lists the *d*-spacing values for the samples. The d_1 values for ABC and ASD were significantly ($P<0.05$) lower than those for MBC and MSD, while MCC showed the lowest d_1 value. Further, the d_2 values for ABC and ASD were significantly ($P<0.05$) higher than those for MBC and MSD, while MCC showed the highest d_2 value. These changes are ascribed to the reduced Iα fraction due to the acid treatment, since Iα is preferentially degraded by acid. Because, the d_1 value for Iα was larger than that for Iβ, and the d_2 value for Iα was smaller than that for Iβ. On the contrary, d_3 was nearly constant owing to the almost same *d*-spacings for Iα and Iβ (Hult et al., 2003; Wada & Okano, 2001; Wada, Okano, & Sugiyama, 1997).

By employing the discriminant analysis developed by Wada et al. (2001), it is possible to categorize cellulose as Iα-rich or Iβ-rich, where $Z>0$ indicates Iα-rich and $Z<0$ indicates Iβ-rich. The *Z*-values for the samples are listed in Table 1. ABC, ASD, and MCC showed $Z<0$; in contrast, MBC and MSD displayed $Z>0$, indicating that they contain more Iα than ABC, ASD, and MCC. These results are in agreement with FT-IR results.

The crystallite sizes CS_1, CS_2, and CS_3 were calculated from 1 0 1, 1 0 $\bar{1}$, and 0 0 2 lattice planes, respectively, and the results are listed in Table 1. ABC, ASD, and MCC showed significantly ($P<0.05$) smaller CS_3 values than MBC and MSD; moreover, MCC showed significantly ($P<0.05$) smaller CS_3 value than ABC and ASD. However at 1 0 1 and 1 0 $\bar{1}$ planes, reliable peaks for MCC could not be obtained, and thus, the FWHM (full-width at half-maximum) values could not be calculated. This was due to the lower intensity of these peaks. It should be noted that the decrease in the mass fraction of Iα is correlated with reduction in crystallite size. It has been reported that Iα tends to crystallize in wider microfibrils, whereas Iβ has a tendency to preferentially form smaller microfibrils (Yamamoto, Horii, & Hirai, 1996).

3.3. SEM analysis

The SEM micrographs of the samples are shown in Fig. 3. MBC and ABC displayed irregular shapes and apparent size dispersity; however, MBC had more elongated particles along with visible asperity. The particle size distribution was difficult to determine accurately because of the irregularity in the particle shapes and overlapping among particles. MBC exhibited particle sizes in the range 10–46 μm; however, MSD showed aggregates of particles with a more granular appearance than their precursor, and the particle sizes were in the range 15–52 μm. ABC displayed a mixture of irregular angular and plate-shaped particles smoother than MBC particles, and the particle sizes in the range 4–23 μm. ASD displayed more regular granular aggregates, with a more spherical appearance than the MBC, MSD, ABC, and MCC particles; the particle sizes for ASD were in the range 8–37 μm. MCC showed a mixture of irregular, elongated, and plate-shaped particles, and irregular aggregate structures with particle sizes in the range 8–67 μm.

3.4. Thermogravimetric analysis (TGA)

TGA and DTG thermograms of the samples are shown in Fig. 4. The broad peaks at 50–180 °C correspond to weight loss due to the evaporation of adsorbed water. The main peaks, observed around 300–400 °C, were attributed to concurrent cellulose degradation processes such as depolymerization, dehydration, and decomposition of glycosyl units, followed by the formation of a charred residue. DTG shows that the degradation temperature, and weight loss for ABC and ASD were higher and lower, respectively, than those for MBC, MSD, and MCC. This result was attributed to the higher crystallinity of ABC and ASD. Furthermore, MCC demonstrated a lower degradation temperature and more weight loss than BC samples. The samples exhibited residual weights of about 9.6%, 12.3%, 13.8%, 19.7%, and 21.2% for MCC, MSD, MBC, ASD, and ABC, respectively. The higher thermal stability of BC than MCC can be ascribed to its distinct ultrafine network structure (Klemm et al., 2006).

3.5. Rheological studies and particle size analysis

The rheograms of ASD, ABC, MSD, and MBC suspensions are shown in Fig. 5. The viscosity significantly ($P<0.05$) increased with concentration increase; however, ABC and ASD exhibited significantly ($P<0.05$) lower viscosity than MBC and MSD. Further, the viscosity as a function of temperature is shown in Fig. 5b. The

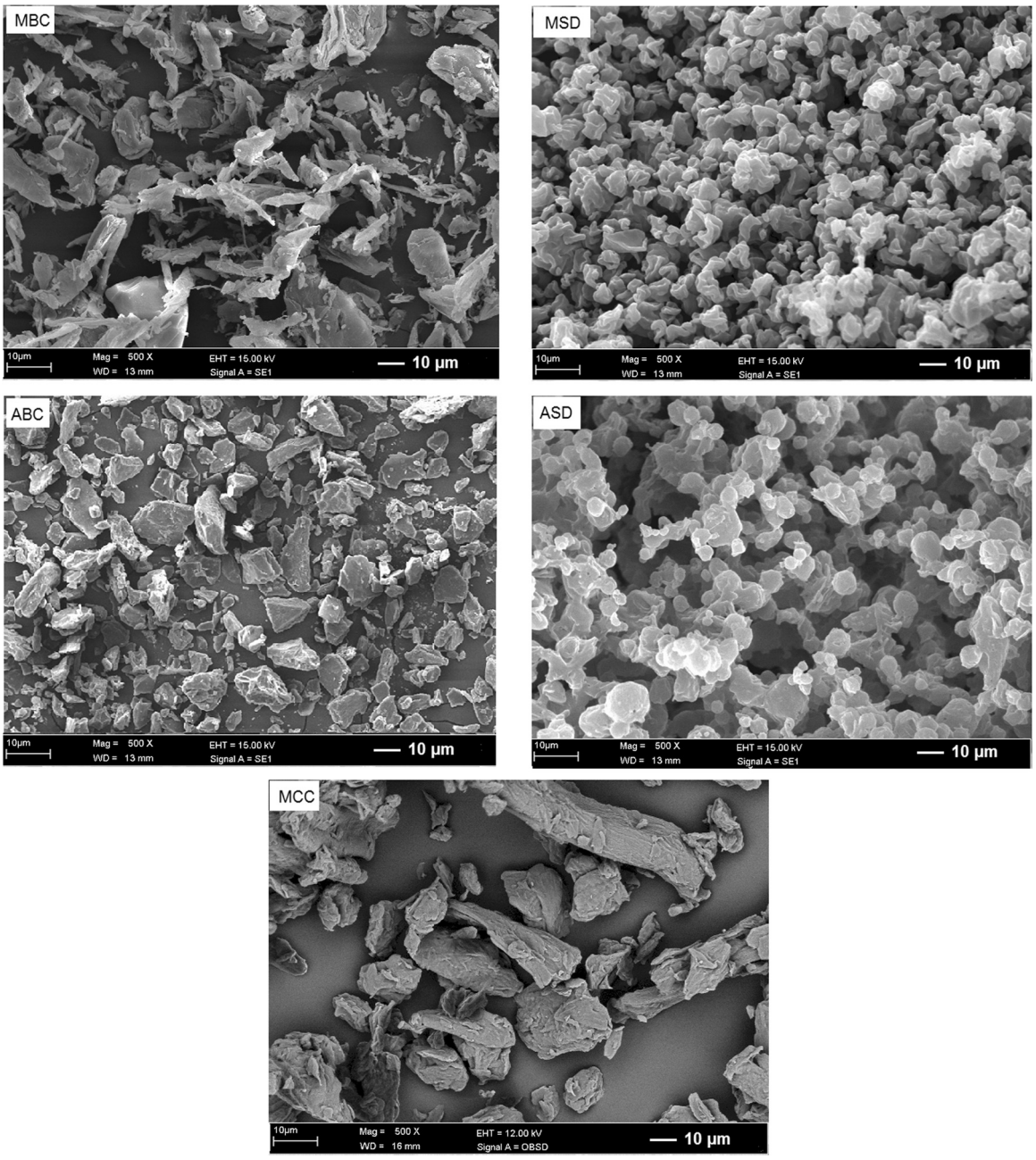

Fig. 3. SEM micrographs of microfine BC (MBC), spray-dried microfine BC (MSD), acid-treated BC (ABC), acid-treated spray-dried BC (ASD), and MCC.

viscosity decreased as the temperature increased; however, MBC and MSD displayed significantly ($P < 0.05$) higher viscosity than ABC and ASD. The effect of temperature on viscosity was more apparent at elevated temperatures of 50 and 60 °C; the viscosity at 60 °C was approximately 17.8%, 18.2%, 30%, and 31.5% lower than that at 25 °C for MBC, MSD, ABC, and ASD, respectively. In general, when external energy is supplied by heating, it increases the energy of the molecules, which in turn, increases the distance between molecules and reduces solution viscosity (Yaşar, Toğrul, & Arslan, 2007). The higher viscosity of MBC and MSD than that of ABC and ASD may be attributed to their particle size and shape: the particles of MBC appeared more elongated with visible asperity, which may have led to greater particles entanglement (Abe & Yano, 2012).

The viscosity as a function of the shear rate for ASD, ABC, MSD, and MBC is depicted in Fig. 5c. The rheograms showed that the viscosity was inversely correlated to the shear rate, which suggests that the samples exhibited shear-thinning flow.

Particle size analysis was employed to determine the ease of redispersal of the spray-dried samples. The $d(0.1)$, $d(0.5)$, and $d(0.9)$ parameters, indicating the percentage of particles 10%, 50%, and 90% possessing diameters equal to or less than the given value, were used in this study to determine the redispersibility of the powders. The results are shown in Fig. 5d. MBC, MSD, ABC, and ASD showed $d(0.5)$ values of around 43.6, 38.9, 24, and 21.8 µm, respectively. Further, MBC, MSD, ABC, and ASD showed $d(0.9)$ values of around 59.1, 53.8, 37.4, and 33.9 µm, respectively, and the trend was similar to that observed for $d(0.5)$. The results showed that MSD and ASD had slightly smaller particles than their precursors. However, the $d(0.1)$, $d(0.5)$, and $d(0.9)$ values for ABC in comparison with those for ASD, as well as the values for MBC in comparison with those for MSD were statistically insignificant ($P > 0.05$).

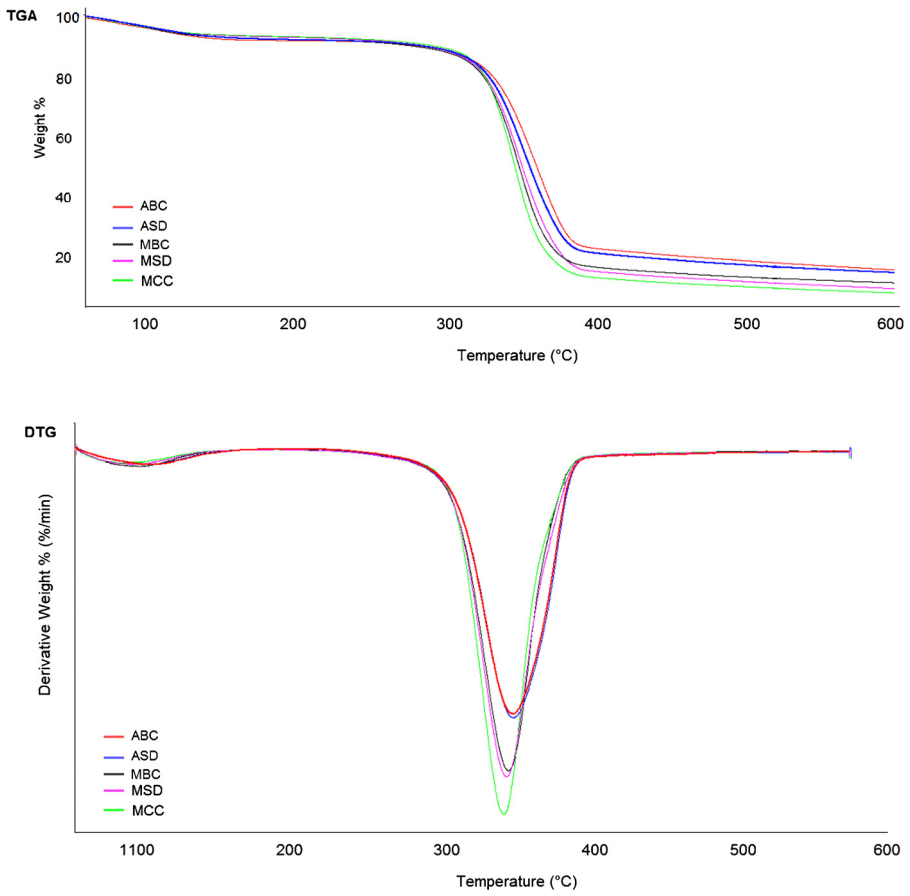

Fig. 4. TGA and DTG thermograms of microfine BC (MBC), spray-dried microfine BC (MSD), acid-treated BC (ABC), acid-treated spray-dried BC (ASD), and MCC.

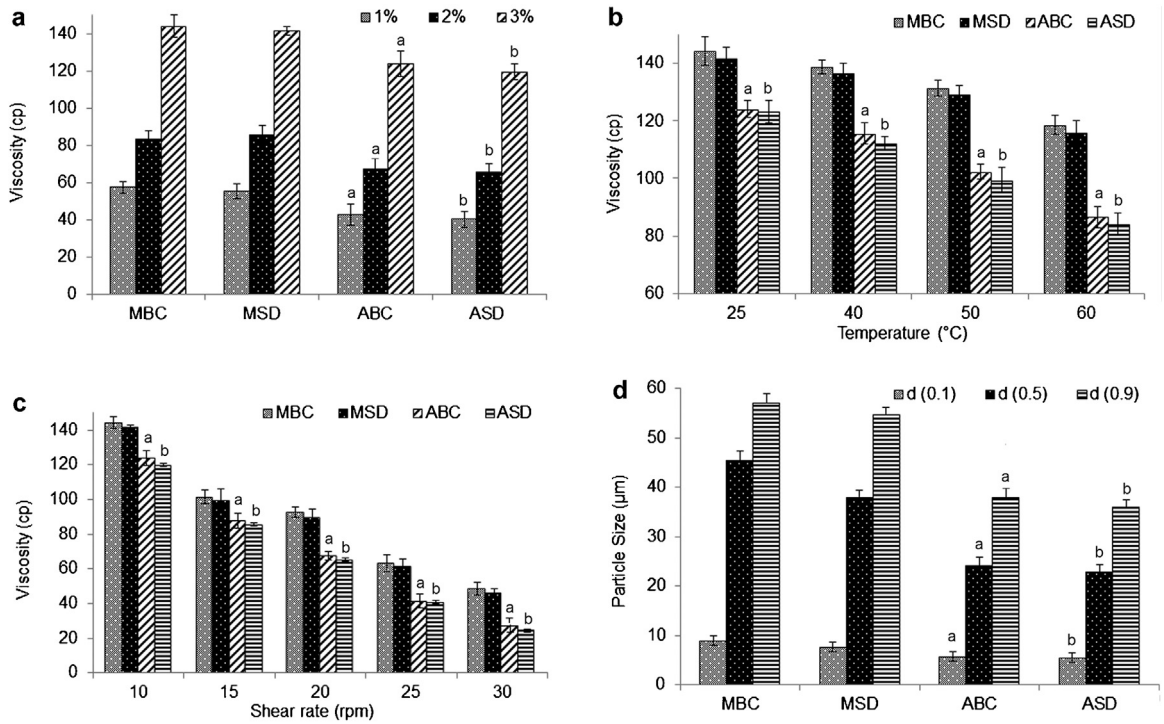

Fig. 5. (a) Effect of percent concentrations on viscosity; (b) effect of temperature on viscosity; (c) effect of shear rate on viscosity; and (d) particle size distributions for microfine BC (MBC), spray-dried microfine BC (MSD), acid-treated BC (ABC), and acid-treated spray-dried BC (ASD). Values are shown as mean ± SD ($n = 3$); $P < 0.05$; [a] Statistically showed significant difference for ABC vs MBC; [b] Statistically showed significant difference for ASD vs MSD.

Table 2
Powder properties of microfine BC (MBC), spray-dried microfine BC (MSD), acid treated BC (ABC), acid treated spray-dried BC (ASD), and MCC.

	Bulk density (g/cm^3)	Tapped density (g/cm^3)	Hausner ratio	Compressibility index (%)	Moisture content (%)	True density (g/cm^3)
MBC	0.213[a] ± 0.007	0.346[a] ± 0.006	1.62[a] ± 0.08	38.40[a] ± 3.1	4.83[a] ± 0.150	1.550 ± 0.003
ABC	0.241[a,b] ± 0.005	0.371[a,b] ± 0.004	1.53[a,b] ± 0.03	34.09[a] ± 2.8	3.86[a,b] ± 0.110	1.552 ± 0.002
MSD	0.294[a,d] ± 0.006	0.389[a,d] ± 0.005	1.32[d] ± 0.07	24.02[d] ± 2.7	3.93[a,d] ± 0.054	1.554 ± 0.003
ASD	0.315[a,c,e] ± 0.004	0.409[c,e] ± 0.004	1.29[e] ± 0.06	22.80[e] ± 2.4	3.74[a,e] ± 0.102	1.554 ± 0.004
MCC	0.329 ± 0.005	0.418 ± 0.005	1.27 ± 0.05	21.20 ± 3.0	3.50 ± 0.101	1.558 ± 0.003

Data are means ± SD ($n = 3$), $P < 0.05$.
[a] Statistically showed significant difference for MBC, MSD, ABC and ASD vs MCC.
[b] Statistically showed significant difference for ABC vs MBC.
[c] Statistically showed significant difference for ASD vs MSD.
[d] Statistically showed significant difference for MSD vs MBC.
[e] Statistically showed significant difference for ASD vs ABC.

Span defines the polydispersity of the particle size. A small span value indicates a narrow particle size distribution; as the span decreases, the polydispersity decreases and the distribution tends to become uniform (Kumar et al., 2013). MBC, MSD, ABC, and ASD showed polydispersity index (PDI) values of 1.34 ± 0.02, 1.29 ± 0.02, 1.19 ± 0.03, and 1.15 ± 0.02, respectively. The PDI values suggest that all powders had a moderate size distribution (Li, Rudolph, Weigl, & Earl, 2004). However, MBC showed a wider size distribution than ABC, while ASD exhibited a narrower size distribution than MSD, which may be attributed to the difference in the shape of primary particles (particles of MBC compared with ABC), which is in agreement with SEM results. The PDI values for ABC in comparison with those for ASD, as well as the values for MBC in comparison with those for MSD were statistically insignificant ($P > 0.05$). These results suggest that no major irreversible agglomeration was ensued and the spray-dried powders could be redispersed, possibly because of the hydrophilicity and high porosity of BC that can enhance water penetration (Eyholzer et al., 2010).

3.6. Powder density and porosity

The powders densities are listed in Table 2. ASD and MSD exhibited significantly ($P < 0.05$) higher bulk and tapped densities than ABC and MBC. Furthermore, ABC displayed significantly ($P < 0.05$) higher densities than MBC. The better packing properties were attributed to the particle shape and size, as ABC displayed smoother and less-elongated particles than MBC, which resulted in better packing. However, MCC displayed higher densities than BC samples, and it can be attributed to the higher porosity of BC (Guo & Catchmark, 2012). The true density values showed no significant difference ($P > 0.05$) between the samples.

Powder porosity is an important characteristic for its performance such as volume reduction during tablet compression, disintegration, and hence, drug release. The porosity values of the powders are listed in Table 3. MSD and ASD had lower porosity than their primary particles, i.e., MBC and ABC, respectively. The more spherical shape and less asperity features resulted in easier packing for MSD and ASD, and hence, their porosities were reduced (Rojas & Kumar, 2011b). However, MCC displayed lower porosity than BC samples; this was ascribed to the higher inter- and intraparticulate porosity of BC (Guo & Catchmark, 2012).

The moisture content of a powder has an impact on its properties as density and flowability, which inevitably influence its performance. For example, if the moisture content is high, caking may occur and the flowability will be reduced. However, if there is sufficient moisture content to cover the surface of the particles, the water acts as a lubricant and the flowability of the powder increases because of friction reduction (Wu, Hung, Miguelez-Moran, Gururajan, & Seville, 2010). Table 2 lists the moisture content values for the powders. MSD and ASD exhibited significantly ($P < 0.05$) lower moisture content than their precursors. However, ABC and ASD showed lower moisture content than MBC and MSD; this was mainly due to the higher crystallinity (Kothari, Kumar, & Banker, 2002). Further, MCC demonstrated significantly ($P < 0.05$) lower moisture content than BC samples; this may be attributed to the higher surface area and porosity of BC resulting from its ultrafine microfibrillar structure (Guo & Catchmark, 2012).

3.7. Powder flowability

Hausner ratio (HR) and compressibility index (CI) have been widely used to estimate the flow properties of powders. A HR value less than 1.20 is indicative of good flowability, whereas a value of 1.50 or higher suggests poor flow (Haware, Tho, & Bauer-Brandl, 2009; Kumar, Kothari, & Banker, 2001). Table 2 shows that MBC and ABC showed HR values of 1.62 and 1.53, respectively, which is indicative of poor flowability, compared with MSD and ASD which showed lower HR values.

A CI index value higher than 26 indicates poor flow. The CI values of the powders are listed in Table 2. MSD and ASD displayed CI values less than 26, whereas MBC and ABC exhibited CI values higher than 26. Further, MCC displayed lower HR and CI values than BC samples; this was mainly due to the difference in their densities,

Table 3
Powder properties of microfine BC (MBC), spray-dried microfine BC (MSD), acid treated BC (ABC), acid treated spray-dried BC (ASD), and MCC.

	Porosity (%)	Flow through an orifice (g s^{-1})	Angle of repose (°)	Swelling index (ml/g)	Water retention capacity (g/g)
MBC	77.76 ± 3.8	0.243[a] ± 0.12	43.5[a] ± 3.3	3.82[a] ± 0.23	3.80[a] ± 0.23
MSD	76.09 ± 2.3	2.970[a,d] ± 0.26	26.4[a,d] ± 3.0	3.64[a] ± 0.40	3.24[a] ± 0.47
ABC	74.81 ± 3.7	0.315[a,b] ± 0.10	37.7[a,b] ± 2.3	3.57[a] ± 0.41	2.87[a,b] ± 0.35
ASD	73.62 ± 2.9	4.230[a,c,e] ± 0.18	21.5[a,c,e] ± 2.5	3.49[a] ± 0.26	2.51[a,c] ± 0.23
MCC	73.41 ± 2.6	0.521 ± 0.13	32.7 ± 3.2	2.60 ± 0.23	2.16 ± 0.34

Data are means ± SD ($n = 3$), $P < 0.05$.
[a] Statistically showed significant difference for MBC, MSD, ABC and ASD vs MCC.
[b] Statistically showed significant difference for ABC vs MBC.
[c] Statistically showed significant difference for ASD vs MSD.
[d] Statistically showed significant difference for MSD vs MBC.
[e] Statistically showed significant difference for ASD vs ABC.

as discussed earlier, since these parameters were calculated from bulk and tapped densities.

The angle of repose provides a qualitative assessment of powder flow. An angle up to 40° indicates reasonable flow potential (Bhimte & Tayade, 2007). Table 3 lists the angle of repose values for the powders. MSD and ASD displayed angles less than 40°, and these values were lower than those for MBC, ABC, and MCC, indicating higher flowability.

The flow rate of a material through an orifice is a direct measure of powder flowability. The flow rate values of the powders are listed in Table 3. MSD and ASD displayed significantly ($P < 0.05$) higher flow rates than their precursors (MBC and ABC, respectively) and MCC. The lower flowability of MBC, ABC, and MCC was mainly caused by their irregular, elongated, and plate-like particles, which resulted in greater interparticle contact areas and interlocking. In general, it can be concluded that the particle shape contributed significantly to the flowability and overall flow of the powders (Bhimte & Tayade, 2007; Villanova, Ayres, & Oréfice, 2011).

3.8. Water retention capacity (WRC) and swelling index (SI)

Water absorption and retention of a powder determines its performance in a product. For example, swelling is one mechanism of disintegrants action, and water retention capability is a prerequisite for excipients to be used in extrusion/spheronization process. Table 3 shows that BC powders had significantly ($P < 0.05$) higher WRC than MCC. However, ABC and ASD exhibited significantly ($P < 0.05$) lower WRC than MBC and MSD, whereas MSD and ASD exhibited slightly lower WRC than their precursors.

The SI values are listed in Table 3. MBC and MSD displayed higher SI than ABC, ASD, and MCC, which was ascribed to their lower crystallinity. Moreover, MSD and ASD exhibited insignificant ($P > 0.05$) lower SI than their precursors. The lower WRC and SI values of ASD and MSD than their primary particles may be attributed to the shrinkage or collapse of some capillary structures as a result of fast water evaporation during spray drying (Tokuyasu, Tabuse, Miyamoto, Matsuki, & Yoza, 2008).

4. Conclusions

BC was prepared from a readily available foodstuff, namely, *nata de coco*. FT-IR analysis revealed that BC is chemically similar to MCC and is satisfactorily pure. Iα content in BC was significantly reduced by acid treatment. SEM images showed that spray drying of BC produced granular microparticles that were more spherical than their precursors and MCC, which significantly enhanced the physical properties and flowability of the powders. Acid treatment of BC led to the formation of smaller particles with less asperity than mechanically prepared particles; this also resulted in some improvement in the physical properties of the powders. TGA analysis showed that BC had higher thermal stability than MCC. Particle size analysis displayed that spray-dried BC powders can be redispersed. BC suspensions showed non-Newtonian shear thinning flow; however, the suspensions prepared from acid-treated powders exhibited lower viscosity than mechanically processed powders. Further, BC powders displayed higher water retention capacity and swelling index than MCC. These results suggest that spray drying of acid-treated and mechanically processed BC powder improves its physical properties. These results provide new insights on the potential applications of spray-dried BC powders as promising pharmaceutical excipients.

Acknowledgment

The authors would like to thank the Ministry of Science, Technology, and Innovation, Malaysia (05-01-02-SF1023) for their financial assistance and support.

References

Abe, K., & Yano, H. (2012). Cellulose nanofiber-based hydrogels with high mechanical strength. *Cellulose*, *19*, 1907–1912.
Amin, M. C. I. M., & Abadi, A. G. (2012). Bacterial cellulose film coating as drug delivery system: Physicochemical. *Thermal and Drug Release Properties. Sains Malaysiana*, *41*(5), 561–568.
Atalla, R. H., & Vanderhart, D. L. (1984). Native cellulose: A composite of two distinct crystalline forms. *Science*, *223*(4633), 283–285.
Bhimte, N. A., & Tayade, P. T. (2007). Evaluation of microcrystalline cellulose prepared from sisal fibers as a tablet excipient: A technical note. *AAPS PharmSciTech*, *8*(1), 56–62.
Cal, K., & Sollohub, K. (2010). Spray drying technique. I: Hardware and process parameters. *Journal of Pharmaceutical Sciences*, *99*(2), 575–586.
Czaja, W., Krystynowicz, A., Bielecki, S., & Brown, J. R. M. (2006). Microbial cellulose—The natural power to heal wounds. *Biomaterials*, *27*(2), 145–151.
Dayal, M. S., Goswami, N., Sahai, A., Jain, V., Mathur, G., & Mathur, A. (2013). Effect of media components on cell growth and bacterial cellulose production from Acetobacter aceti MTCC 2623. *Carbohydrate Polymers*, *94*(1), 12–16.
Edgar, K. J. (2007). Cellulose esters in drug delivery. *Cellulose*, *14*(1), 49–64.
Eyholzer, C., Bordeanu, N., Lopez-Suevos, F., Rentsch, D., Zimmermann, T., & Oksman, K. (2010). Preparation and characterization of water-redispersible nanofibrillated cellulose in powder form. *Cellulose*, *17*(1), 19–30.
George, J., Ramana, K., & Bawa, A. (2011). Bacterial cellulose nanocrystals exhibiting high thermal stability and their polymer nanocomposites. *International Journal of Biological Macromolecules*, *48*(1), 50–57.
George, J., & Siddaramaiah. (2012). High performance edible nanocomposite films containing bacterial cellulose nanocrystals. *Carbohydrate Polymers*, *87*, 2031–2037.
Guo, J., & Catchmark, J. M. (2012). Surface area and porosity of acid hydrolyzed cellulose nanowhiskers and cellulose produced by Gluconacetobacter xylinus. *Carbohydrate Polymers*, *87*(2), 1026–1037.
Halib, N., Amin, M., & Ahmad, I. (2010). Unique stimuli responsive characteristics of electron beam synthesized bacterial cellulose/acrylic acid composite. *Journal of Applied Polymer Science*, *116*, 2920–2929.
Halib, N., & Amin, M. C. I. M. (2012). Physicochemical properties and characterization of nata de coco from local food industries as a source of cellulose. *Sains Malaysiana*, *41*(2), 205–211.
Haware, R. V., Tho, I., & Bauer-Brandl, A. (2009). Application of multivariate methods to compression behavior evaluation of directly compressible materials. *European Journal of Pharmaceutics and Biopharmaceutics*, *72*(1), 148–155.
Hayashi, N., Sugiyama, J., Okano, T., & Ishihara, M. (1997). Selective degradation of the cellulose Iα component in Cladophora cellulose with Trichoderma viride cellulase. *Carbohydrate Research*, *305*(1), 109–116.
Heinze, T., Schwikal, K., & Barthel, S. (2005). Ionic liquids as reaction medium in cellulose functionalization. *Macromolecular Bioscience*, *5*(6), 520–525.
Hult, E. L., Iversen, T., & Sugiyama, J. (2003). Characterization of the supermolecular structure of cellulose in wood pulp fibres. *Cellulose*, *10*(2), 103–110.
Klemm, D., Schumann, D., Kramer, F., Heßler, N., Hornung, M., Schmauder, H. P., et al. (2006). Nanocelluloses as innovative polymers in research and application. *Advances in Polymer Science*, *205*, 49–96.
Kolakovic, R., Laaksonen, T., Peltonen, L., Laukkanen, A., & Hirvonen, J. (2012). Spray-dried nanofibrillar cellulose microparticles for sustained drug release. *International Journal of Pharmaceutics*, *430*(1–2), 47–55.
Kothari, S. H., Kumar, V., & Banker, G. S. (2002). Comparative evaluations of powder and mechanical properties of low crystallinity celluloses, microcrystalline celluloses, and powdered celluloses. *International Journal of Pharmaceutics*, *232*(1), 69–80.
Kumar, B., Sharma, V., & Pathak, K. (2013). Effect of melt sonocrystallization on pharmacotechnical properties of paracetamol, indomethacin and mefenamic acid characterized by dynamic laser scattering and its impact on solubility. *Drug Development and Industrial Pharmacy*, *39*(5), 687–695.
Kumar, V., Kothari, S., & Banker, G. (2001). Compression, compaction, and disintegration properties of low crystallinity celluloses produced using different agitation rates during their regeneration from phosphoric acid solutions. *AAPS PharmSciTech*, *2*(2), 22–28.
Lan, W., Liu, C. F., Yue, F.-X., Sun, R. C., & Kennedy, J. F. (2011). Ultrasound-assisted dissolution of cellulose in ionic liquid. *Carbohydrate Polymers*, *86*(2), 672–677.
Lee, K. Y., & Bismarck, A. (2012). Susceptibility of never-dried and freeze-dried bacterial cellulose towards esterification with organic acid. *Cellulose*, *19*(3), 891–900.
Li, Q., Rudolph, V., Weigl, B., & Earl, A. (2004). Interparticle van der Waals force in powder flowability and compactibility. *International Journal of Pharmaceutics*, *280*(1–2), 77–93.
Müller, A., Ni, Z., Hessler, N., Wesarg, F., Müller, F. A., Kralisch, D., et al. (2013). The biopolymer bacterial nanocellulose as drug delivery system: Investigation of drug loading and release using the model protein albumin. *Journal of Pharmaceutical Sciences*, *102*(2), 579–592.
Panesar, P. S., Chavan, Y., Chopra, H. K., & Kennedy, J. F. (2012). Production of microbial cellulose: Response surface methodology approach. *Carbohydrate Polymers*, *87*(1), 930–934.
Park, S., Baker, J. O., Himmel, M. E., Parilla, P. A., & Johnson, D. K. (2010). Cellulose crystallinity index: Measurement techniques and their impact on interpreting cellulase performance. *Biotechnology for Biofuels*, *3*(10), 1–10.
Paudel, A., Worku, Z. A., Meeus, J., Guns, S., & Van den Mooter, G. (2013). Manufacturing of solid dispersions of poorly water soluble drugs by spray drying:

Formulation and process considerations. *International Journal of Pharmaceutics*, *453*(1), 253–284.
Peng, Y., Gardner, D. J., & Han, Y. (2012). Drying cellulose nanofibrils: In search of a suitable method. *Cellulose*, *19*, 91–102.
Rojas, J., & Kumar, V. (2011a). Assessment of processing and polymorphic form effect on the powder and tableting properties of microcrystalline celluloses I and II. *International Journal of Research in Pharmaceutical Sciences*, *2*(2), 276–284.
Rojas, J., & Kumar, V. (2011b). Comparative evaluation of silicified microcrystalline cellulose II as a direct compression vehicle. *International Journal of Pharmaceutics*, *416*, 120–128.
Ruka, D. R., Simon, G. P., & Dean, K. M. (2012). Altering the growth conditions of Gluconacetobacter xylinus to maximize the yield of bacterial cellulose. *Carbohydrate Polymers*, *89*(2), 613–622.
Satyamurthy, P., Jain, P., Balasubramanya, R. H., & Vigneshwaran, N. (2011). Preparation and characterization of cellulose nanowhiskers from cotton fibres by controlled microbial hydrolysis. *Carbohydrate Polymers*, *83*(1), 122–129.
Tokuyasu, K., Tabuse, M., Miyamoto, M., Matsuki, J., & Yoza, K. (2008). Pretreatment of microcrystalline cellulose flakes with CaCl2 increases the surface area, and thus improves enzymatic saccharification. *Carbohydrate Research*, *343*(7), 1232–1236.
Tomé, L. C., Brandão, L., Mendes, A. M., Silvestre, A. J., Neto, C. P., Gandini, A., et al. (2010). Preparation and characterization of bacterial cellulose membranes with tailored surface and barrier properties. *Cellulose*, *17*(6), 1203–1211.
Ul-Islam, M., Shah, N., Ha, J. H., & Park, J. K. (2011). Effect of chitosan penetration on physico-chemical and mechanical properties of bacterial cellulose. *Korean Journal of Chemical Engineering*, *28*(8), 1736–1743.
Villanova, J., Ayres, E., & Oréfice, R. (2011). Design of prolonged release tablets using new solid acrylic excipients for direct compression. *European Journal of Pharmaceutics and Biopharmaceutics*, *79*(3), 664–673.
Wada, M., & Okano, T. (2001). Localization of Iα and Iβ phases in algal cellulose revealed by acid treatments. *Cellulose*, *8*(3), 183–188.
Wada, M., Okano, T., & Sugiyama, J. (1997). Synchrotron-radiated X-ray and neutron diffraction study of native cellulose. *Cellulose*, *4*(3), 221–232.
Wada, M., Okano, T., & Sugiyama, J. (2001). Allomorphs of native crystalline cellulose I evaluated by two equatorial *d*-spacings. *Journal of Wood Science*, *47*(2), 124–128.
Walton, D., & Mumford, C. (1999). Spray dried products—Characterization of particle morphology. *Chemical Engineering Research and Design*, *77*(1), 21–38.
Wu, C. Y., Hung, W. L., Miguelez-Moran, A., Gururajan, B., & Seville, J. (2010). Roller compaction of moist pharmaceutical powders. *International Journal of Pharmaceutics*, *391*(1), 90–97.
Yamamoto, H., Horii, F., & Hirai, A. (1996). In situ crystallization of bacterial cellulose II. Influences of different polymeric additives on the formation of celluloses Iα and Iβ at the early stage of incubation. *Cellulose*, *3*(1), 229–242.
Yan, Z., Chen, S., Wang, H., Wang, B., & Jiang, J. (2008). Biosynthesis of bacterial cellulose/multi-walled carbon nanotubes in agitated culture. *Carbohydrate Polymers*, *74*(3), 659–665.
Yaşar, F., Toğrul, H., & Arslan, N. (2007). Flow properties of cellulose and carboxymethyl cellulose from orange peel. *Journal of Food Engineering*, *81*(1), 187–199.